



Article

Electrochemical Micro-Immunosensor of Cubic AuPt Dendritic Nanocrystals/Ti₃C₂-MXenes for Exosomes Detection

Wenpo Feng ^{1,2}, Pingping Xu ², Mei Wang ², Guidan Wang ², Guangda Li ² and Aihua Jing ^{2,*}¹ Medical College, Pingdingshan University, Pingdingshan 467000, China² School of Medical Technology and Engineering, Henan University of Science and Technology, Luoyang 471023, China

* Correspondence: aihuj@haust.edu.cn; Tel.: +86-0379-64162573

Abstract: Exosomes are extracellular vesicles that exist in body circulation as intercellular message transmitters. Although the potential of tumor-derived exosomes for non-invasive cancer diagnosis is promising, the rapid detection and effective capture of exosomes remains challenging. Herein, a portable electrochemical aptasensor of cubic AuPt dendritic nanocrystals (AuPt DNs)/Ti₃C₂ assisted in signal amplification, and aptamer CD63 modified graphene oxide (GO) was immobilized on a screen-printed carbon electrode (SPCE) as the substrate materials for the direct capture and detection of colorectal carcinoma exosomes. Cubic AuPt DNs/Ti₃C₂ was synthesized according to a simple hydrothermal procedure, and the AuPt DNs/Ti₃C₂-Apt hybrid demonstrated an efficient recognition of exosomes. Under optimal conditions, a detection limit of down to 20 exosomes μL^{-1} was achieved with the linear range from 100 exosomes μL^{-1} to 5.0×10^5 exosomes μL^{-1} . The proposed immunosensor could be suitable for the analysis of exosomes and has clinical value in the early diagnosis of cancer.

Keywords: immunosensor; cubic AuPt dendritic nanocrystals; MXenes; exosomes



Citation: Feng, W.; Xu, P.; Wang, M.; Wang, G.; Li, G.; Jing, A. Electrochemical Micro-Immunosensor of Cubic AuPt Dendritic Nanocrystals/Ti₃C₂-MXenes for Exosomes Detection. *Micromachines* **2023**, *14*, 138. <https://doi.org/10.3390/mi14010138>

Academic Editor: Liang He

Received: 20 November 2022

Revised: 23 December 2022

Accepted: 31 December 2022

Published: 4 January 2023



Copyright: © 2023 by the authors. Licensee MDPI, Basel, Switzerland. This article is an open access article distributed under the terms and conditions of the Creative Commons Attribution (CC BY) license (<https://creativecommons.org/licenses/by/4.0/>).

1. Introduction

Malignant tumors are dangerous to human health due to their high morbidity and mortality. The non-invasive early diagnosis of malignant tumors has attracted attention to improve the survival rates of patients in clinical research. Exosomes, lipid-membrane-bound nanovesicles [1,2], have attracted much attention for early cancer screening technologies to provide intercellular communication with large numbers of macromolecules involving specific proteins, lipids, DNA, mRNA, and microRNAs [3]. Exosomes act as a potential tumor biomarker, which is one of the most efficient prognostic indicators for early cancer diagnosis in clinical research [4,5]. They are derived from tumor cells and mediate messages between donor cells and recipient cells, and alter immune response regulation and intracellular bioactive molecule transmission [6].

Several quantitative methods, such as enzyme-linked immunosorbent analysis [7], dynamic light scattering [8], flow cytometry [9], and nanoparticle tracking [10], have been reported for recognizing and detecting exosomes. These methods can detect exosome concentration and size as well as provide new pathways for extracellular vesicles; they can provide further utility due to their special structures and functions. However, they all have limitations such as complicated procedures, long detection time, and the difficulty in quantifying smaller exosomes. New detection techniques, such as colorimetry, fluorescence, and electrochemical techniques, have been developed for exosome identification and measurement [11–13]. Among these strategies, biosensors have been regarded as a valuable analytical platform in many fields, especially in the detection and monitoring of disease diagnosis and treatment, displaying the advantages of being highly selective, providing fast responses, high sensitivity [14,15], and efficient use of the analyte. The use of biosensors has attracted

much attention in terms of the reorganization and detection of tumor markers, including exosomes [16]. Specifically, electrochemical immunosensors based on nanomaterials with excellent performances conjugated with aptamers for signal amplification represent an outstanding method that can quantify biomarkers in clinical diagnosis [17,18]. Nonetheless, the signal amplification of the immunosensors for exosome detection is based on the interface of the modified electrode. A high immobilizing efficiency of the biorecognition layer and a superior nanocarrier are of critical importance for increasing the sensitivity of an immunosensor. Therefore, nanomaterials that provide a rapid electric response are urgently needed.

MXenes, with a new two-dimensional (2D) transition metal carbide, layered transition metal carbide, nitride, or carbonitride, have attracted increased attention in recent years in the field of electrochemical sensors, supercapacitors, ion batteries, and liquid biopsies [19,20]. Ti_3C_2 , as the earliest discovered MXenes material, is also the most widely used with superior properties such as excellent electron transfer, highly catalytic activity, good biocompatibility, and large surface areas. Moreover, their special nanostructure and excellent conductivity make MXenes and MXenes/metal nanoparticle hybrids potential materials for the fabrication of biosensors [21,22]. Cubic AuPt dendritic nanocrystals (AuPt DNs), with excellent electrocatalytic activity and excellent biocompatibility, have been used as substrate materials for capturing antibodies in immunosensors. Wu et al. developed a biosensor based on the amino functionalization of Ti_3C_2 MXene for the detection of tumor biomarkers [23]. In addition, due to the abundant oxygen or hydroxyl terminated surface, Ti_3C_2 can interact with a majority of biomolecules in many ways, which make them unique nanobiointerface units for biosensor construction [24]. Therefore, AuPt DNs combined with Ti_3C_2 MXene were used as the matrix nanoprobe to selectively and reproducibly detect exosomes, and AuPt DNs showed excellent catalytic and conductive properties.

The quantitative detection of exosomes with electrochemical biosensors could be determined using antibodies as recognition molecules [25]. Aptamers, an attractive alternative to antibodies, played a key role in the determination of exosomes in recent years by binding to desired targets with excellent specificity, high stability, easy synthesis, and low cost [26]. Li et al. developed an aptasensor based on a hemin/G-quadruplex-assisted signal amplification strategy to perform the electrochemical detection of gastric cancer exosomes [27]. Tan et al. developed an aptamer-based nanotetrahedron-assisted biosensor to capture and detect hepatocellular exosomes [28]. Zhou et al. reported a microfluidic chip electrochemical biosensor based on aptamer recognition for exosome detection. A methylene blue-labeled DNA detection chain hybridizes with the CD63 aptamer, which can be determined with a detection limit of 1×10^6 particles/mL. However, these aptamer-based methods are mostly nonspecific target capture methods, which make it difficult to detect tumor exosomes and nontumor exosomes. Therefore, it is urgently desirable to develop new aptasensors to recognize and detect specific exosomes (e.g., cancerous exosomes) rapidly and easily.

Screen printing technology was used to make on-site and point-of-care biosensors for their easy miniaturization, lower cost, disposable nature, and mass production [29]. A screen-printed carbon electrode (SPCE) is often used, with the fabrication of electrochemical immunosensors, to monitor physiological indicators in the process of diagnosis [30]. In this work, an SPCE was employed to design an electrochemical immunosensor for the efficient detection of colorectal cancer-derived exosomes (Figure 1). First, a CD63-aptamer-modified SPCE was fabricated to capture exosomes owing to its advantages such as simplicity, low cost, small size, rapid responses, and easy mass production. Moreover, the CD63-aptamer-modified cubic AuPt DNs-combined Ti_3C_2 MXene was selected as the matrix material to capture exosomes. The characterization of the TEM, XRD, and SEM of cubic AuPt DNs displayed the specific nanostructures of cubic AuPt DNs, which expose more active sites and, therefore, enhance the high sensitivity of the immunosensor. The optimization of detection conditions (such as the incubation time, the Apt concentration, and the concentration of KCL) for the detection of exosomes was performed. The linear range of the sensor

is $100\text{--}5 \times 10^5$ exosomes / μL , and the detection limit is 20 exosomes / μL ($S/N = 3$). The developed immunosensor was tested for exosome detection in human serum samples, which can provide a new promising method to create a miniaturized portable potentiostat working with microvolumes and for point-of-care analysis in clinical settings.

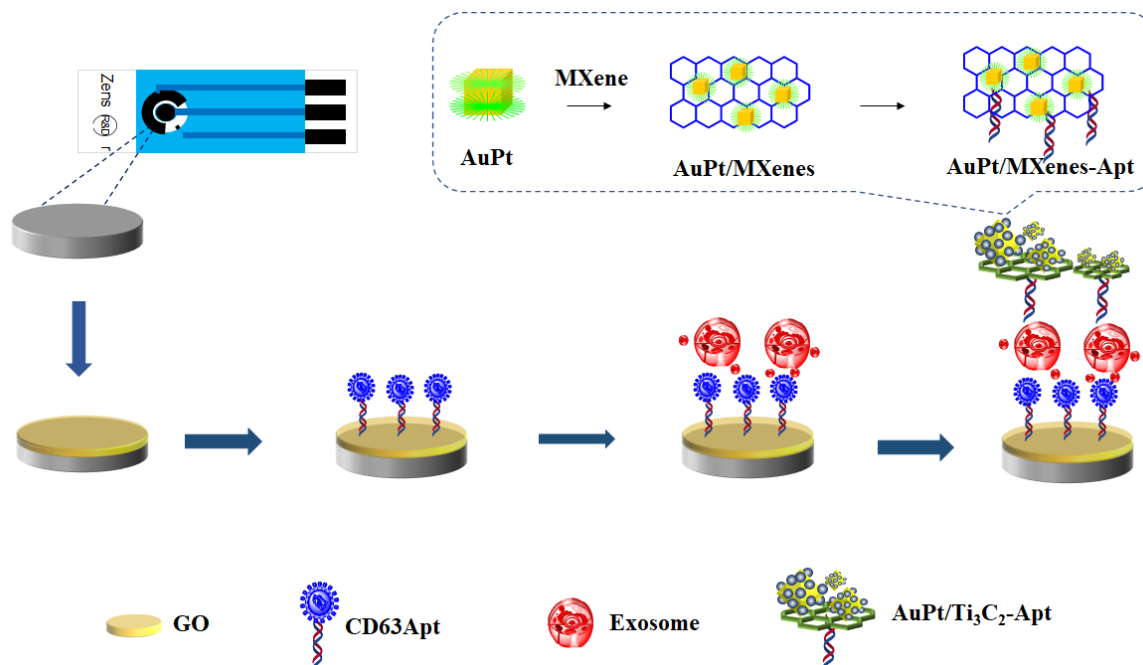


Figure 1. The schematic illustration of the fabrication procedure of the exosome electrochemical biosensor.

2. Materials and Methods

The main fabrication of the sandwich-type electrochemical biosensor is the synthesis of Ti₃C₂ MXenes, cubic Au/Pt DNs, and Au/Pt/Ti₃C₂ MXenes, which we performed as described below.

2.1. Reagents and Materials

Hydrogen fluoride acid was purchased from Tianjin Fuyu Fine Chemical Co., Ltd. (Tianjin, China). Ti₃AlC₂ was purchased from Shandong Diyan New Material Technology Co., Ltd. (Heze, China). Glycine (Gly) was from Tianjin Fengchuan Chemical Reagent Technology Co., Ltd. (Tianjin, China). N-Hydroxysuccinimide sodium salt (NHS) and 1-Ethyl-3-(3-dimethylaminopropyl) carbodiimide hydrochloride (EDC) were from Tianjin BASF chemical company (Tianjin, China). DMEM medium (high glucose), HAuCl₄, and CD63 Apt were obtained from Sangon Biotech (Shanghai, China) Co., Ltd. Potassium ferricyanide (K₃Fe(CN)₆), potassium ferrocyanide (K₄Fe(CN)₆), and KCl were supplied by Tianjin Bodie Chemical Co., Ltd. (Tianjin, China).

2.2. Apparatus and Characterization

The X-ray diffraction (XRD) patterns were collected using a D8 ADVANCE X-ray diffractometer. The transmission electron microscopy (TEM) images were obtained with a JEOL 2010 transmission electron microscope. A JEOL 5160LV electron microscope was used to acquire scanning electron microscopy (SEM) images. Electrochemical detection was performed on disposable screen-printed electrodes (SPCEs) with a 3 mm diameter working area (Zensor research & development, Taiwan) connected with a CHI 660E workstation (Chenhua, Shanghai, China).

2.3. Cell Culture, Exosome Extraction, and Counting

HCT116 human colon cancer cell lines (HCT-1165FR) obtained from the American Type Culture Collection were maintained in MacCoy's 5A medium (Invitrogen, Carlsbad, CA, USA) supplemented with 10% fetal bovine serum (FBS) (GIBCOBRL Laboratories, Grand Island, NY, USA) and 1% penicillomycin into DMEM in a humidified incubator at 37 °C in an atmosphere of 5% CO₂ (Thermo Scientific, Waltham, MA, USA) [31]. When the cell concentration reached about 70%, the culture medium was replaced with a serum-free medium. After 24 h, the cell medium was collected and exosomes were separated by performing differential centrifugation. The specific steps were as follows: The culture medium (300 mL) was centrifuged at 500× *g* (*g* represents gravitational acceleration) for 15 min, and the supernatant was collected. The supernatant was centrifuged at 2000× *g* for 20 min and filtrated by membrane. The precipitates were then centrifuged at 3000× *g* for 15 min twice and 100,000× *g* for 90 min, before being collected and dispersed in PBS solution. Exosomes were stored at −20 °C for further use. The particle size distribution of exosomes was measured with the Malvern particle size analyzer, and the results showed that the size of exosomes was about 120 nm. The concentration of exosomes was determined with the BCA method, and the results show that the concentration of exosomes was 2.2×10^9 exosomes /μL.

2.4. Synthesis of Ti₃C₂ MXenes

The multilayered Ti₃C₂T_X was synthesized using the HF etching method according to a previously reported procedure with simple modification [32,33]. A total of 1 g of Ti₃AlC₂ powder and 20 mL of HF (40 wt%) solution was mixed at 0 °C and stirred for 10 min. The above mixture was then stirred at 35 °C for 24 h until the reaction was completed. After that, the mixture was centrifuged at a speed of 8000 rpm and washed with deionized water until the pH was no less than 6. The precipitate Ti₃C₂ MXene was dispersed in deionized water by performing ultrasound and freeze-dried for 12 h.

2.5. Preparing Au/Pt DNs

The Au/Pt DNs were prepared according to a previously published method [34]. Firstly, 10 mL of HAuCl₄ (0.25 mM) and CTAB (75 mM) aqueous solution were prepared in a flask, following which 0.6 mL of ice NaBH₄ (10 mM) solution was rapidly injected, and stirred slowly for 3 h. Then, the hydrosol prepared at 1 mL was diluted to 100 mL and used as the seed solution. The colorless mixture of 0.1 mL HAuCl₄ (10 mM), 2 mL CTAB (0.2 M), and 1.5 mL AA (ascorbic acid) (0.1 M) was diluted to 25 mL, and 0.3 mL of the prepared seed solution was added. The reaction mixture was shaken at room temperature for 8 h and a colloid containing pale purple cubic gold was obtained. Finally, AuPt DNs were prepared by adding 2 mL AA (0.1 M) and 1 mL H₂PtCl₆ (10 mM) to the third gold solution, successively, and washed with ultra-pure water at 60 °C for 12 h.

2.6. Synthesis of Au/Pt/Ti₃C₂ MXene

The Au/Pt/Ti₃C₂ MXene nanocomposite was synthesized as follows [35]: Under ultrasonic conditions, Ti₃C₂ MXene powder and Au/Pt powder were dispersed in DMF solution. Next, the DMF solution of Au/Pt and Ti₃C₂ MXene were mixed together and ultrasonicated for 3 h. The mixed solution was further stirred for 20 h. The Au/Pt/Ti₃C₂ MXene was collected by performing centrifugation, washed with DMF and ethanol, and then dried in vacuum at 60 °C for 12 h.

2.7. Preparation of Au/Pt/Ti₃C₂ MXene Nanoprobe

A total of 5 mg of Gly was dissolved in 5 mL of deionized water and stirred at room temperature. Then, 10 mL 1.0 mg/mL Au/Pt-Ti₃C₂ MXene dispersion was added drop by drop, stirred at room temperature for 24 h, centrifuged for washing (12,000 rpm, 20 min), that is, Pt DNS-Ti₃C₂ MXene-Gly was prepared. After 150 μL EDC (400 mM), NHS (100 mM) and 100 μL Aptamer (-COOH) mixtures were activated at 37 °C for 1 h, 200 μL Au/Pt DNS-Ti₃C₂ MXene- St. Louis Gly was added to the above solution, and the reaction

continued for 1 h at 37 °C. Centrifugal washing (1200, 10 min) was performed, as well as deionized water dispersion, for Au/Pt DNS-Ti₃C₂ MXene-GLY-Apt.

2.8. Preparation of Biosensor

Figure 1 shows a schematic of representation of fabrication process of the electrochemical biosensor. This article uses disposable screen-printed electrodes (SPCEs) for detection. In total, 6 µL of GO (0.25 mg/L) was dropped on the cleaned SPCE surface to gain GO/SPCE. After being dried, the electrode was immersed in EDC/NHS(100 µM/300 µM), and incubated at 37 °C for 1 h [36]. The CD63 aptamer stock solution (100 µM) was mixed with 10 mM tris(2-carboxyethyl) phosphine (TCEP, Sigma-Aldrich, St. Louis, MO, USA) for 1 h to cleave the disulfide bonds, and then 4-(2-hydroxyethyl)-1-piperazineethanesulfonic acid (HEPES, Sigma-Aldrich, St. Louis, MO, USA) buffer was used to further dilute the CD63 aptamers to 1 µM. Then, 40 µL of the prepared solution of CD63 aptamers was placed on the microelectrodes for 2 h to obtain Apt/GO/SPCEs. After incubation, the Apt/GO/SPCEs were washed with deionized (DI) water. Next, 30 µL of 1 mM 6-mercapto-1-hexanol (MCH, Sigma-Aldrich, St. Louis, MO, USA) was added to the Apt/GO/SPCEs for 15 min. To remove the excess MCH, the Apt/GO/SPCEs were washed thoroughly with DI water [37]. The Apt/GO/SPCEs were immersed in the exosomes derived from colorectal cells at certain concentrations. Then, the exosomes/Apt/GO/SPCEs were incubated with MXenes-Apt for 2 h at 37 °C.

Subsequently, the electrode that captured the exosomes was placed in a Ti₃C₂-MXene-Apt solution and incubated at 37 °C for 2 h. Then, the cubic AuPt DNS-Ti₃C₂-MXenes-Apt solution was covered on the surface to form cubic AuPt DNS-Ti₃C₂-MXenes-Apt/exosomes/Apt/GO/SPCEs. Finally, the cubic AuPt DNS/Ti₃C₂-MXenes-Apt/exosomes/Apt/GO/SPCEs electrode was ready for testing.

3. Results and Discussion

Electrochemical immunosensors have been a tool in the early monitoring and diagnosis of cancer. Our group demonstrated the use of this method as a label-free detection route of the cancer biomarker by dendritic tri-fan blade-like PdAuCu nanoparticles/aminefunctionalized graphene oxide [30]. In order to obtain a high sensitivity in the electrochemical immunosensors, trimetallic nanomaterials have broad applications due to their excellent properties, e.g., superior catalytic activity, better durability, and larger surface-active areas.

The major accomplishment of this work is detecting potential tumor-biomarker exosomes with nanomaterials of cubic AuPt dendritic nanocrystals/Ti₃C₂. Herein, the electrochemical immunosensor of cubic AuPt dendritic nanocrystals/Ti₃C₂-MXene are reported. The properties of the used materials are displayed first, and the characterization of the immunosensor was followed by its further application in a real sample.

3.1. Characterization of Ti₃C₂ MXenes, Ti₃C₂ MXenes, and Cubic AuPt DNSs/Ti₃C₂ MXenes

The morphological structure of the as-prepared MXene-Ti₃C₂T_x and Ti₃C₂ MXenes was analyzed using SEM. The SEM image of Ti₃AlC₂ (Figure 2A) shows a multilayered structure with a typical accordion-like morphology. Figure 2C shows the morphology of the prepared MXene-Ti₃C₂T_x with thin and transparent nanoflakes stacked on each other. The layer spacing is wider than before the etching [24,25]. The structural characteristics of the as-prepared MXene-Ti₃C₂T_x and Ti₃C₂ MXenes composite structures were investigated by performing XRD analysis, as shown in Figure 2B. Visibly, following etching, the characteristic peak of Ti₃AlC₂ at 39° disappeared [26]. This proves that MXene-Ti₃C₂T_x was successfully prepared. In the pattern of Ti₃C₂ MXenes, the sharp peak located at ≈32° can be assigned to Ti₃C₂T_x, confirming the existence of Ti₃C₂T_x support [22]. The high-resolution TEM (HRTEM) image reveals a highly crystalline lattice of the MXene basal plane without evident defects (Figure 2D), which is consistent with a previous report on MXene nanosheets prepared using LiF-HCl etchant.

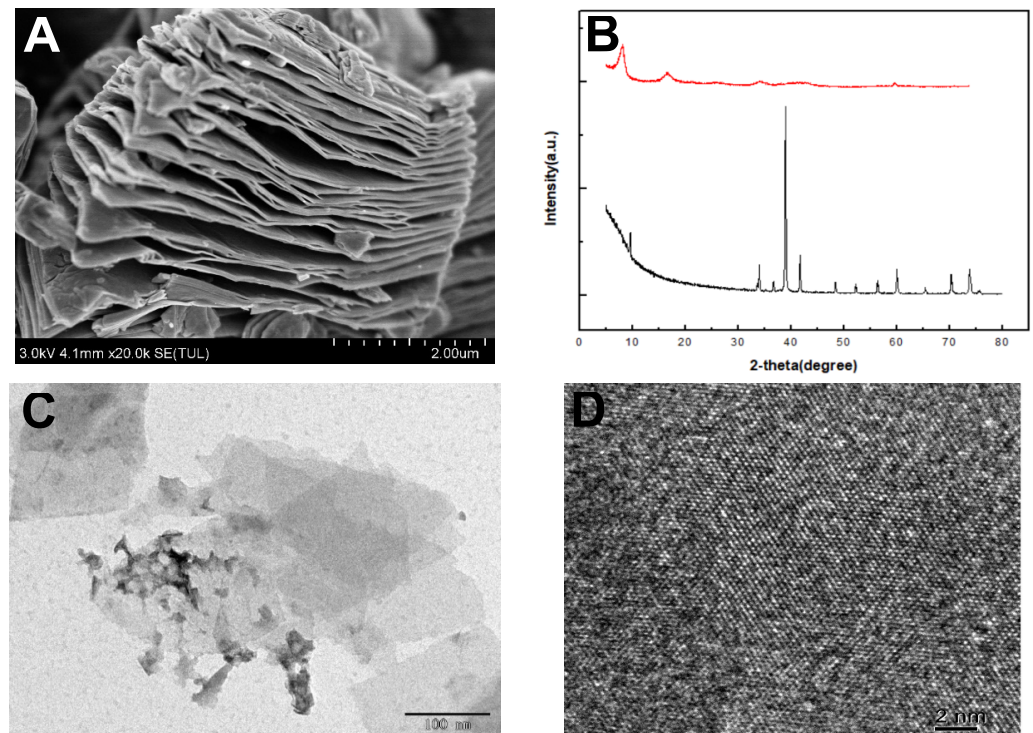


Figure 2. SEM (A), X-ray diffraction (XRD) patterns (B), TEM images (C), and HRTEM image (D) of the MXene $\text{Ti}_3\text{C}_2\text{T}_x$.

TEM was used to characterize Au, cubic AuPt DNPs, and cubic AuPt- Ti_3C_2 MXene. Figure 3A shows the TEM images of cubic Au, indicating that the obtained Au NPs have formed a cubic morphology with an average size of 30 nm. Figure 3B shows the diffraction pattern of cubic Au, which further confirms the successful preparation of cubic Au. Figure 3C shows the TEM image of AuPt DNPs, indicating that AuPt DNPs form a highly uniform dendrite form with a regular size. Figure 3D shows a visible modification of cubic AuPt DNPs on the Ti_3C_2 MXene lamellar, which proves the successful preparation of the composite materials.

3.2. Electrochemical Characterizations of the Assembly Processes of the Biosensor

CV and EIS were used to study the modified process of the electrochemical biosensor. Figure 4A shows the CVs of $[\text{Fe}(\text{CN})_6]^{3-}/[\text{Fe}(\text{CN})_6]^{4-}$ in PBS using the bare (curve a), GO modified (curve b), GO/Apt (curve c), GO/Apt/exosomes (curve d), and GO/Apt/exosome/ Ti_3C_2 -Apt-cubic AuPt DNPs (curve e) modified SPCEs. The changes in the amperometric response correspond to the obstruction of the electron transfer kinetics of the $\text{Fe}(\text{CN})_6^{3-}/\text{Fe}(\text{CN})_6^{4-}$ probe. An electrochemical signal was detected using bare SPCEs, as shown in curve a. When GO and Apt composite materials (curves b/c) are modified on SPCEs, the peak current after modification of GO and Apt gradually decreases due to the electronic inertness. After exosomes are loaded, due to the specific binding of exosomes and aptamers, the peak current is further reduced. Due to the electronic inertness of Apt and exosomes, the electron transfer of the substrate ions on the electrode interface is hindered. Therefore, after Ti_3C_2 MXene modification, the peak current will also decrease. Due to the negative charge of GO, the transfer of the substrate at the electrode interface was blocked, resulting in a further reduction in the peak current.

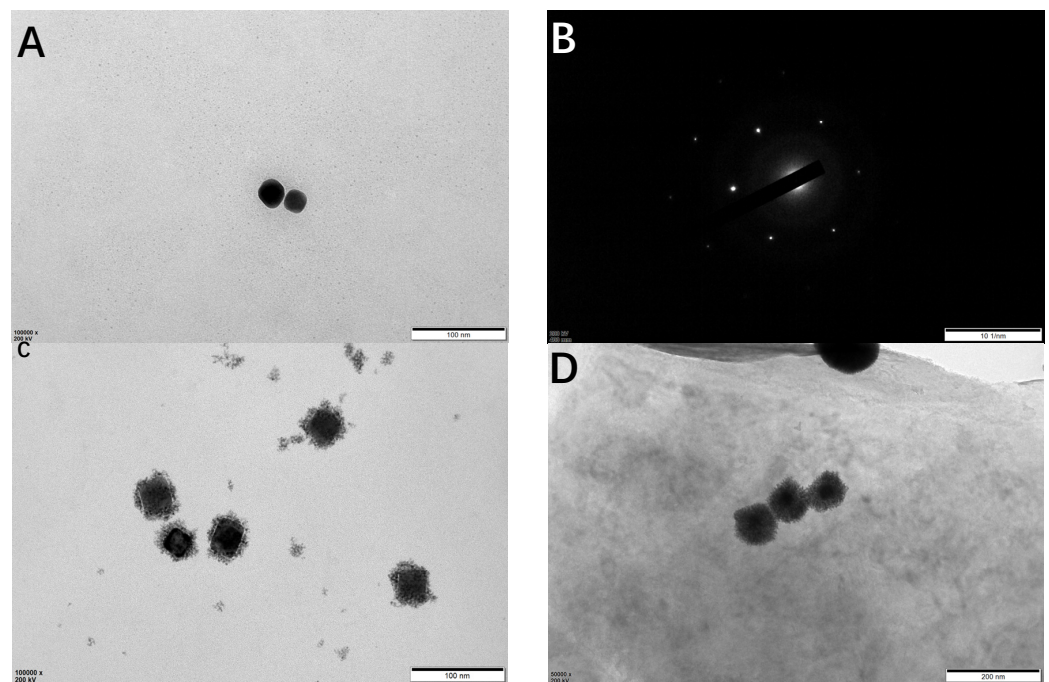


Figure 3. TEM images of cubic Au (A), diffraction pattern of cubic Au (B), Au@Pt DNs (C), and Au/Pt DNs-Ti₃C₂ MXene (D).

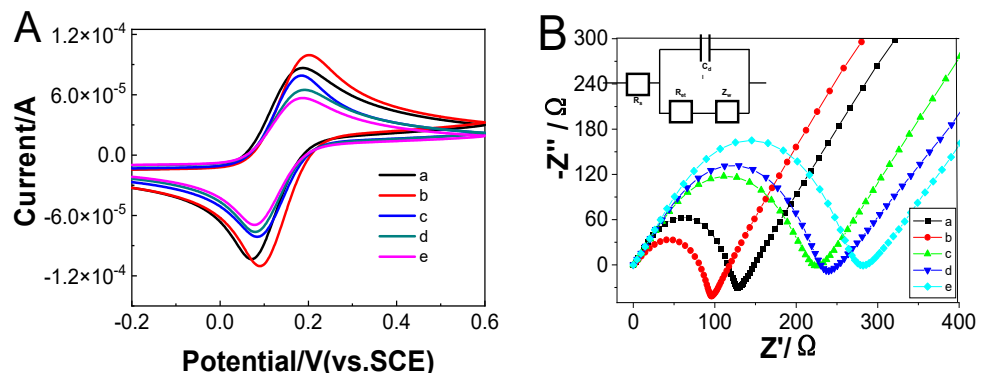


Figure 4. (A) CVs and (B) nyquist plots of bare (a) SPCEs, GO (b), Apt/GO (c), exosome/Apt/GO (d), cubic AuPt DN-Ti₃C₂-Apt/exosome/Apt/GO (e) modified SPCEs in 0.10 M KCl containing 5.0×10^{-3} M K₃[Fe(CN)₆]/K₄[Fe(CN)₆].

The EIS measurement was more sensitive in monitoring the changes in the interface features in the [Fe(CN)₆]³⁻/[Fe(CN)₆]⁴⁻ probes system of the modified electrodes. Figure 4B is the EIS diagram of the modified electrode. The impedance spectrum of EIS is divided into two parts, a semicircular part and a linear part. The semicircle part represents the electron transfer process, and the diameter of the semicircle is equal to the electron transfer resistance; the linear part corresponds to the diffusion process. After the electrode surface is assembled, the resistance increases, and the obtained result corresponds to the CV diagram, which proves that the sensor is successfully assembled.

3.3. Optimization of the Detection Conditions

In order to obtain the best analytical performance of the biosensor, the influence of the incubation time of the exosomes, the concentration of Apt, and the concentration of KCL in the substrate were detected. It can be seen from Figure 5A that the performance of this biosensor is related to the incubation time of the exosomes. The optimal incubation time of

the exosomes, as shown in Figure 5A, is 120 min, when the peak current is the largest. For this reason, a 120 min incubation time was used in the following experiments.

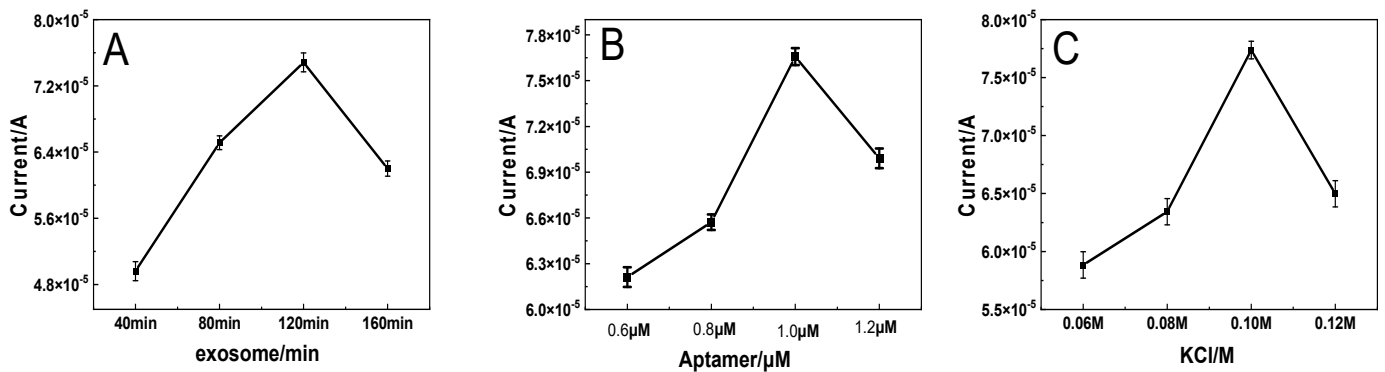


Figure 5. Effect of (A) the incubation time, (B) the Apt concentration, and (C) the concentration of KCL on the DPV response during the detection of exosomes.

The concentration of Apt also affects the performance of this biosensor. As shown in Figure 5B, when the concentration of Apt increased from 0.6 μ M to 1.0 μ M, the peak current gradually increased and did not change drastically when the Apt concentration exceeded 1.0 μ M. This result shows that when the concentration of Apt is under 1.0 μ M, there is not enough Apt to combine the exosome; when the concentration of Apt is 1.0 μ M, Apt reaches the point of saturation on the surface of the exosome, and the ability to combine exosomes is optimal. Therefore, 1.0 μ M of Apt was used for electrochemical measurement [23].

In addition, the performance of the biosensor is also related to the concentration of KCL in the substrate (Figure 5C). Before the concentration of KCL in the base solution is 0.10 M, the peak current increases, which is conducive to the transfer of electrons; however, if the concentration exceeds this, the peak current will appear to decrease, which is not conducive to the transfer of electrons. Therefore, 0.10 M KCL was used for the preparation of the biosensors.

3.4. The Sensitivity of the Biosensor

The designed electrochemical biosensor was used in this study strategy to detect exosomes through the DPV response curve under optimal conditions. Figure 6A illustrates the electrochemical signal intensity of the biosensor in different concentrations of colorectal cancer cell exosome solutions. These curves, from curve a to curve h in Figure 6A, represent the current responses of the as-prepared immunosensor incubated with different concentration of exosomes: 1.0×10^2 , 5.0×10^2 , 1.0×10^3 , 2.5×10^3 , 1.0×10^4 , 2.5×10^4 , 5.0×10^4 , and 5.0×10^5 exosomes μ L $^{-1}$.

At the same time, it can be seen that the current response increases as the concentration of exosomes increased. Figure 6B shows the relationship between the logarithm of the exosome concentration and the current corresponding with what was shown in Figure 6A, and the peak current height was linear with the logarithm of the exosomes concentration in the range from 100 to 5.0×10^5 exosomes μ L $^{-1}$. The linear regression equation is $I = 1.726 \times 10^{-5} \log C + 1.420 \times 10^{-5}$ (exosomes μ L $^{-1}$), and the correlation coefficient is 0.9971. The detection limit is 20 exosomes μ L $^{-1}$ (S/N = 3). These data show that this biosensor can be used to detect exosomes with high sensitivity. Table 1 shows the comparison between the proposed electrochemical biosensor and other technologies in the electrochemical detection of exosomes. These comparisons indicated that this method is significantly better than other similar methods. This explains that the designed biosensor has good signal amplification performance.

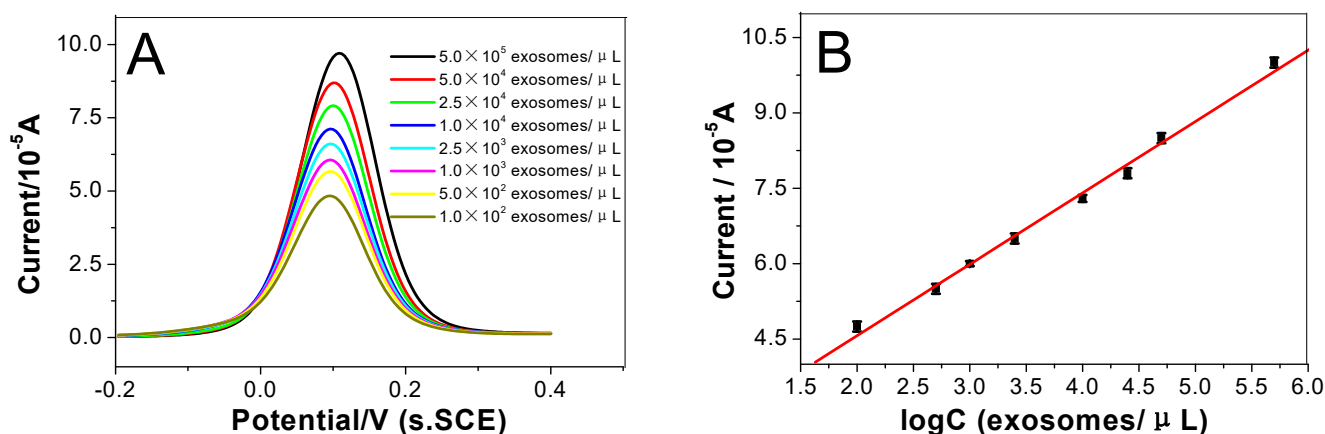


Figure 6. (A) DPV responses of the proposed immunosensor after incubation with various concentrations of exosomes in $[\text{Fe}(\text{CN})_6]^{4-}/3^-$. (From down to top, concentrations of exosomes are: 1.0×10^2 , 5.0×10^2 , 1.0×10^3 , 2.5×10^3 , 1.0×10^4 , 2.5×10^4 , 5.0×10^4 , 5.0×10^5 exosomes μL^{-1}); (B) Linear relationship between the current I of the immunosensor and logarithm of exosome concentration. Error bars represent the standard deviation, $n = 5$.

Table 1. Comparison of the response characteristics of various modified electrodes.

Method	Detection Range (Particles μL^{-1})	Detection Limit (Particles μL^{-1})	Refs.
Electrochemical method	5×10^2 – 5×10^5	229	[38]
Electrogenerated chemiluminescence	10^2 – 10^5	30	[39]
Energy transfer	10^4 – 10^9	1.4×10^3	[40]
Electrochemical method	10^3 – 1.2×10^5	70	[41]
Electrochemical method	1×10^2 – 1×10^6	2×10^2	[42]
Electrochemical method	100 – 5×10^5	20	This work

3.5. Specificity and Reproducibility of the Sensor

Specificity is an important parameter of electrochemical biosensors. The specificity between aptamers and exosomes was analyzed. As shown in Figure 7A, the peak current without exosomes and random Apt is lower than under normal conditions. This is because the colorectal cancer exosomes are incubated in the exosome solution, so that the exosomes are captured on the electrode; therefore, more cubic AuPt DNs-Ti₃C₂-Apt nanoprobe can be modified on the electrode to generate a larger current signal. At the same time, it can also be attributed to the modification of the CD63 aptamer on the electrode to capture more exosomes, so that a large number of cubic AuPt DNs-Ti₃C₂-Apt nanoprobe are modified on the electrode to generate a stronger current. These results show that this biosensor has good specificity. Figure 7B shows the reproducibility test of the immunosensor. Specifically, five immunosensors fabricated independently were applied to detect the target exosome (5.0×10^3 exosomes μL^{-1}) under the optimized conditions. The relative standard deviation (RSD) was approximately 2.8%, displaying acceptable reproducibility.

3.6. Detection of Cancerous Exosomes Isolated from Human Serum Samples

In order to investigate the practical application of the proposed electrochemical biosensor in biological samples, different concentrations of colorectal-derived exosomes were added to the serum for measurement. The experimental results detected are shown in Table 2, and the recoveries were in the range of 98–108%. This indicates that the developed electrochemical sensor has high accuracy in the detection of exosomes in complex samples.

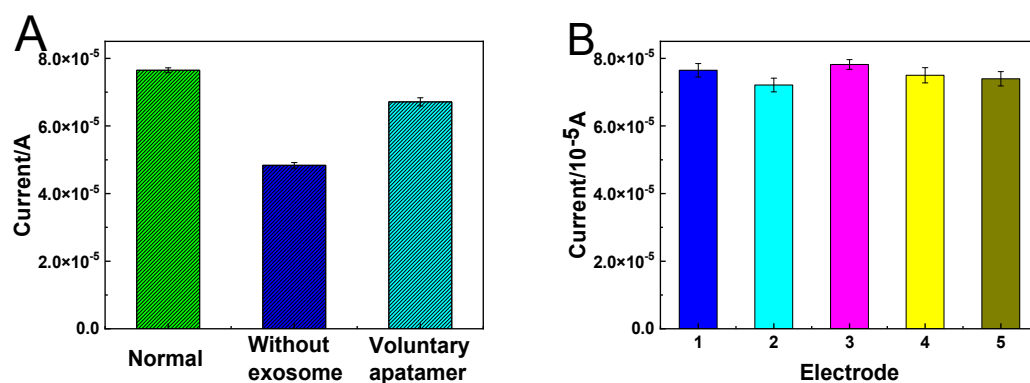


Figure 7. (A) Study of the specificity of the electrochemical biosensor toward various interferences. Error bars represent standard deviation, $n = 5$. The concentration of exosomes was 5.0×10^3 exosomes μL^{-1} . (B) Electrochemical responses of five immunosensor fabricated independently.

Table 2. The detection results of exosomes in serum using the biosensor.

Sample Number	Added (Log Exosome μL^{-1})	Found (Log Exosomes μL^{-1})	Recovery (%)
1	3	3.16	105
2	3.5	3.43	98
3	4	4.35	108
4	4.5	4.47	99
5	5	5.02	100

4. Conclusions

In summary, an MXene electrochemical biosensor platform based on cubic AuPt DNs-Ti₃C₂ MXene was built for the detection of exosomes using an aptamer-assisted amplification strategy. The GO/SPEC interface modified by the CD63 aptamer can specifically bind to the CD63 protein on the surface of exosomes to improve their capture ability. Ti₃C₂ can specifically bind to a large number of CD63 aptamers and can efficiently recognize exosomes and serve as nanocarriers. The cubic AuPt DNs-Ti₃C₂ MXene-Apt hybrid also improves electrocatalytic activity. The fabricated electrode shows a wider linear detection range of $100 \sim 5.0 \times 10^5$ exosomes μL^{-1} with a limit of detection of as low as 20 exosomes μL^{-1} . In addition, this method can also be effectively applied to detect exosomes in complex serum samples. It is believed that the design of the functionalized MXene membranes expands possibilities for the implementation of 2D membrane platforms for reliable biomarker diagnosis and for the monitoring of clinical applications, such as tumor cell-promoting miRNA detection, tumor cell/exosome enrichment, and drug screening.

Author Contributions: W.F. and P.X. contributed equally to this work; conceptualization, W.F. and A.J.; methodology, P.X.; writing—original draft preparation, P.X.; writing—review and editing, M.W.; visualization, G.W.; project administration, G.L. All authors have read and agreed to the published version of the manuscript.

Funding: The present study was funded by the Natural Science Foundation of China under grant numbers U2004137 and U1304805, the Henan Province Scientific and Technology Research Project, the Natural Science Foundation of Henan Province (numbers 222102310437 and 202300410150), and High Level Talent Startup Foundations of Pingdingshan University (PXY-BSQD-202009).

Data Availability Statement: The data of this work are available from the corresponding author upon reasonable request.

Conflicts of Interest: The authors declare no conflict of interest.

References

1. Jin, D.; Yang, F.; Zhang, Y.; Liu, L.; Zhou, Y.; Wang, F.; Zhang, G.-J. ExoAPP: Exosome-Oriented, Aptamer Nanoprobe-Enabled Surface Proteins Profiling and Detection. *Anal. Chem.* **2018**, *90*, 14402–14411. [[CrossRef](#)]
2. Sanchez-Reyes, L.-M.; Rodriguez-Resendiz, J.; Salazar-Colores, S.; Nelida Avecilla-Ramirez, G.; Israel Perez-Soto, G. A High-Accuracy Mathematical Morphology and Multilayer Perceptron-Based Approach for Melanoma Detection. *Appl. Sci.* **2020**, *10*, 1098. [[CrossRef](#)]
3. Yang, Y.; Kannisto, E.; Yu, G.; Reid, M.E.; Patnaik, S.K.; Wu, Y. An Immuno-Biochip Selectively Captures Tumor-Derived Exosomes and Detects Exosomal RNAs for Cancer Diagnosis. *ACS Appl. Mater. Interfaces* **2018**, *10*, 43375–43386. [[CrossRef](#)]
4. Zhang, X.; Liu, C.; Pei, Y.; Song, W.; Zhang, S. Preparation of a Novel Raman Probe and Its Application in the Detection of Circulating Tumor Cells and Exosomes. *ACS Appl. Mater. Interfaces* **2019**, *11*, 28671–28680. [[CrossRef](#)]
5. Wang, J.; Li, W.; Zhang, L.; Ban, L.; Chen, P.; Du, W.; Feng, X.; Liu, B.-F. Chemically Edited Exosomes with Dual Ligand Purified by Microfluidic Device for Active Targeted Drug Delivery to Tumor Cells. *ACS Appl. Mater. Interfaces* **2017**, *9*, 27441–27452. [[CrossRef](#)]
6. Zhang, Y.; Jiao, J.; Wei, Y.; Wang, D.; Yang, C.; Xu, Z. Plasmonic Colorimetric Biosensor for Sensitive Exosome Detection via Enzyme-Induced Etching of Gold Nanopyramid@MnO₂ Nanosheet Nanostructures. *Anal. Chem.* **2020**, *92*, 15244–15252. [[CrossRef](#)]
7. Shin, H.; Jeong, H.; Park, J.; Hong, S.; Choi, Y. Correlation between Cancerous Exosomes and Protein Markers Based on Surface-Enhanced Raman Spectroscopy (SERS) and Principal Component Analysis (PCA). *ACS Sens.* **2018**, *3*, 2637–2643. [[CrossRef](#)]
8. Liu, C.; Xu, X.; Li, B.; Situ, B.; Pan, W.; Hu, Y.; An, T.; Yao, S.; Zheng, L. Single-Exosome-Counting Immunoassays for Cancer Diagnostics. *Nano Lett.* **2018**, *18*, 4226–4232. [[CrossRef](#)]
9. Song, F.; Wang, C.; Wang, C.; Gao, J.; Liu, H.; Zhang, Y.; Han, L. Enrichment-Detection Integrated Exosome Profiling Biosensors Promising for Early Diagnosis of Cancer. *Anal. Chem.* **2021**, *93*, 4697–4706. [[CrossRef](#)]
10. Chen, J.; Xu, Y.; Lu, Y.; Xing, W. Isolation and Visible Detection of Tumor-Derived Exosomes from Plasma. *Anal. Chem.* **2018**, *90*, 14207–14215. [[CrossRef](#)]
11. Liang, G.; Zhu, Y.; Ali, D.J.; Tian, T.; Xu, H.; Si, K.; Sun, B.; Chen, B.; Xiao, Z. Engineered exosomes for targeted co-delivery of miR-21 inhibitor and chemotherapeutics to reverse drug resistance in colon cancer. *J. Nanobiotechnol.* **2020**, *18*, 10. [[CrossRef](#)]
12. Li, S.; Ma, Q. Electrochemical nano-sensing interface for exosomes analysis and cancer diagnosis. *Biosens. Bioelectron.* **2022**, *214*, 114554. [[CrossRef](#)]
13. Jiang, Y.; Shi, M.; Liu, Y.; Wan, S.; Cui, C.; Zhang, L.; Tan, W. Aptamer/AuNP Biosensor for Colorimetric Profiling of Exosomal Proteins. *Angew. Chem. Int. Ed.* **2017**, *56*, 11916–11920. [[CrossRef](#)]
14. Dong, H.; Chen, H.; Jiang, J.; Zhang, H.; Cai, C.; Shen, Q. Highly Sensitive Electrochemical Detection of Tumor Exosomes Based on Aptamer Recognition-Induced Multi-DNA Release and Cyclic Enzymatic Amplification. *Anal. Chem.* **2018**, *90*, 4507–4513. [[CrossRef](#)]
15. Wang, J.; Huang, X.; Xie, J.; Han, Y.; Huang, Y.; Zhang, H. Exosomal analysis: Advances in biosensor technology. *Clin. Chim. Acta* **2021**, *518*, 142–150. [[CrossRef](#)]
16. Yu, X.; Sha, L.; Dong, L.; Cao, Y.; Zhao, J. Recent Advances in Bio-Sensing Methods for the Detection of Tumor Exosomes. *Crit. Rev. Anal. Chem.* **2022**, *52*, 356–374. [[CrossRef](#)]
17. Zhao, H.; Lin, Q.; Huang, L.; Zhai, Y.; Liu, Y.; Deng, Y.; Su, E.; He, N. Ultrasensitive chemiluminescence immunoassay with enhanced precision for the detection of cTnI amplified by acridinium ester-loaded microspheres and internally calibrated by magnetic fluorescent nanoparticles. *Nanoscale* **2021**, *13*, 3275–3284. [[CrossRef](#)]
18. Fang, Y.; Liu, H.; Wang, Y.; Su, X.; Jin, L.; Wu, Y.; Deng, Y.; Li, S.; Chen, Z.; Chen, H.; et al. Fast and Accurate Control Strategy for Portable Nucleic Acid Detection (PNAD) System Based on Magnetic Nanoparticles. *J. Biomed. Nanotechnol.* **2021**, *17*, 407–415. [[CrossRef](#)]
19. Iravani, S.; Varma, R.S. MXenes for Cancer Therapy and Diagnosis: Recent Advances and Current Challenges. *ACS Biomater. Sci. Eng.* **2021**, *7*, 1900–1913. [[CrossRef](#)]
20. Pang, J.; Mendes, R.G.; Bachmatiuk, A.; Zhao, L.; Ta, H.Q.; Gemming, T.; Liu, H.; Liu, Z.; Rummeli, M.H. Applications of 2D MXenes in energy conversion and storage systems. *Chem. Soc. Rev.* **2019**, *48*, 72–133. [[CrossRef](#)]
21. Kalambate, P.K.; Dhanjai, Sinha, A.; Li, Y.; Shen, Y.; Huang, Y. An electrochemical sensor for ifosfamide, acetaminophen, domperidone, and sumatriptan based on self-assembled MXene/MWCNT/chitosan nanocomposite thin film. *Microchim. Acta* **2020**, *187*, 402. [[CrossRef](#)]
22. Yang, X.; Ga, N.; Zhou, S.; Zhao, J. MXene nanoribbons as electrocatalysts for the hydrogen evolution reaction with fast kinetics. *Phys. Chem. Chem. Phys.* **2018**, *20*, 19390–19397. [[CrossRef](#)]
23. Wu, Q.; Li, N.; Wang, Y.; Xu, Y.; Wu, J.; Jia, G.; Ji, F.; Fang, X.; Chen, F.; Cui, X. Ultrasensitive and Selective Determination of Carcinoembryonic Antigen Using Multifunctional Ultrathin Amino-Functionalized Ti₃C₂-MXene Nanosheets. *Anal. Chem.* **2020**, *92*, 3354–3360. [[CrossRef](#)]
24. You, Q.; Zhuang, L.; Chang, Z.; Ge, M.; Mei, Q.; Yang, L.; Dong, W.F. Hierarchical Au nanoarrays functionalized 2D Ti₂CT_x MXene membranes for the detection of exosomes isolated from human lung carcinoma cells. *Biosens. Bioelectron.* **2022**, *216*, 114647. [[CrossRef](#)]

25. Zhu, C.; Li, L.; Wang, Z.; Irfan, M.; Qu, F. Recent advances of aptasensors for exosomes detection. *Biosens. Bioelectron.* **2020**, *160*, 112213. [[CrossRef](#)]
26. Ding, X.; Mauk, M.G.; Yin, K.; Kadimisetty, K.; Liu, C. Interfacing Pathogen Detection with Smartphones for Point-of-Care Applications. *Anal. Chem.* **2019**, *91*, 655–672. [[CrossRef](#)]
27. Huang, R.; He, L.; Xia, Y.; Xu, H.; Liu, C.; Xie, H.; Wang, S.; Peng, L.; Liu, Y.; Liu, Y.; et al. A Sensitive Aptasensor Based on a Hemin/G-Quadruplex-Assisted Signal Amplification Strategy for Electrochemical Detection of Gastric Cancer Exosomes. *Small* **2019**, *15*, 1900735. [[CrossRef](#)]
28. Wang, S.; Zhang, L.; Wan, S.; Cansiz, S.; Cui, C.; Liu, Y.; Cai, R.; Hong, C.; Teng, I.T.; Shi, M.; et al. Aptasensor with Expanded Nucleotide Using DNA Nanotetrahedra for Electrochemical Detection of Cancerous Exosomes. *ACS Nano* **2017**, *11*, 3943–3949. [[CrossRef](#)]
29. Leng, C.; Wu, J.; Xu, Q.; Lai, G.; Ju, H.; Yan, F. A highly sensitive disposable immunosensor through direct electro-reduction of oxygen catalyzed by palladium nanoparticle decorated carbon nanotube label. *Biosens. Bioelectron.* **2011**, *27*, 71–76. [[CrossRef](#)]
30. Xu, P.; Feng, W.; Wang, M.; Zhang, L.; Liang, G.; Jing, A. New Ultrasensitive Sandwich-Type Immunoassay of Dendritic Tri-Fan Blade-like PdAuCu Nanoparticles/Amine-Functionalized Graphene Oxide for Label-Free Detection of Carcinoembryonic Antigen. *Micromachines* **2021**, *12*, 1256. [[CrossRef](#)]
31. Jing, A.; Zhang, C.; Liang, G.; Feng, W.; Tian, Z.; Jing, C. Hyaluronate-Functionalized Graphene for Label-Free Electrochemical Cytosensing. *Micromachines* **2018**, *9*, 669. [[CrossRef](#)] [[PubMed](#)]
32. Alhabeib, M.; Maleski, K.; Anasori, B.; Lelyukh, P.; Clark, L.; Sin, S.; Gogotsi, Y. Guidelines for Synthesis and Processing of Two-Dimensional Titanium Carbide ($Ti_3C_2T_x$ MXene). *Chem. Mater.* **2017**, *29*, 7633–7644. [[CrossRef](#)]
33. Naguib, M.; Kurtoglu, M.; Presser, V.; Lu, J.; Niu, J.; Heon, M.; Hultman, L.; Gogotsi, Y.; Barsoum, M.W. Two-Dimensional Nanocrystals Produced by Exfoliation of Ti_3AlC_2 . *Adv. Mater.* **2011**, *23*, 4248–4253. [[CrossRef](#)] [[PubMed](#)]
34. Lv, H.; Li, Y.; Zhang, X.; Gao, Z.; Zhang, C.; Zhang, S.; Dong, Y. Enhanced peroxidase-like properties of Au@Pt DNs/NG/Cu²⁺ and application of sandwich-type electrochemical immunosensor for highly sensitive detection of CEA. *Biosens. Bioelectron.* **2018**, *112*, 1–7. [[CrossRef](#)] [[PubMed](#)]
35. Li, Z.; Zhuang, Z.; Lv, F.; Zhu, H.; Zhou, L.; Luo, M.; Zhu, J.; Lang, Z.; Feng, S.; Chen, W.; et al. The Marriage of the FeN₄ Moiety and MXene Boosts Oxygen Reduction Catalysis: Fe 3d Electron Delocalization Matters. *Adv. Mater.* **2018**, *30*, 1803220. [[CrossRef](#)] [[PubMed](#)]
36. Yang, G.; Lai, Y.; Xiao, Z.; Tang, C.; Deng, Y. Ultrasensitive electrochemical immunosensor of carcinoembryonic antigen based on gold-label silver-stain signal amplification. *Chin. Chem. Lett.* **2018**, *29*, 1857–1860. [[CrossRef](#)]
37. Zhang, W.; Tian, Z.; Yang, S.; Rich, J.; Zhao, S.; Klingeborn, M.; Huang, P.-H.; Li, Z.; Stout, A.; Murphy, Q.; et al. Electrochemical micro-aptasensors for exosome detection based on hybridization chain reaction amplification. *Microsyst. Nanoeng.* **2021**, *7*, 63. [[CrossRef](#)]
38. Wang, Y.; Xu, H.; Luo, J.; Liu, J.; Wang, L.; Fan, Y.; Yan, S.; Yang, Y.; Cai, X. A novel label-free microfluidic paper-based immunosensor for highly sensitive electrochemical detection of carcinoembryonic antigen. *Biosens. Bioelectron.* **2016**, *83*, 319–326. [[CrossRef](#)]
39. Zhao, D.; Wang, Y.; Nie, G. Electrochemical immunosensor for the carcinoembryonic antigen based on a nanocomposite consisting of reduced graphene oxide, gold nanoparticles and poly(indole-6-carboxylic acid). *Microchim. Acta* **2016**, *183*, 2925–2932. [[CrossRef](#)]
40. Norouzi, P.; Gupta, V.K.; Faridbod, F.; Pirali-Hamedani, M.; Larijani, B.; Ganjali, M.R. Carcinoembryonic Antigen Admittance Biosensor Based on Au and ZnO Nanoparticles Using FFT Admittance Voltammetry. *Anal. Chem.* **2011**, *83*, 1564–1570. [[CrossRef](#)]
41. Zhao, L.; Li, J.; Liu, Y.; Wei, Y.; Zhang, J.; Zhang, J.; Xia, Q.; Zhang, Q.; Zhao, W.; Chen, X. A novel ECL sensor for determination of carcinoembryonic antigen using reduced graphene Oxide-BaYF₅:Yb, Er upconversion nanocomposites and gold nanoparticles. *Sens. Actuators B Chem.* **2016**, *232*, 484–491. [[CrossRef](#)]
42. Liu, N.; Ma, Z. Au-ionic liquid functionalized reduced graphene oxide immunosensing platform for simultaneous electrochemical detection of multiple analytes. *Biosens. Bioelectron.* **2014**, *51*, 184–190. [[CrossRef](#)] [[PubMed](#)]

Disclaimer/Publisher's Note: The statements, opinions and data contained in all publications are solely those of the individual author(s) and contributor(s) and not of MDPI and/or the editor(s). MDPI and/or the editor(s) disclaim responsibility for any injury to people or property resulting from any ideas, methods, instructions or products referred to in the content.